Evaluating Yangtze River Delta Urban Agglomeration flood risk using hybrid method of AutoML and AHP

Yu Gao [1,2], Haipeng Lu [1,2], Yaru Zhang[1,2], Hengxu Jin[1,2], Shuai Wu[3], Yixuan Gao[1,2], Shuliang Zhang[1,2*]

1 Key Laboratory of VGE of Ministry of Education, Nanjing Normal University, Nanjing 210023, China

2 Jiangsu Center for Collaborative Innovation in Geographical Information Resource Development and Application, Nanjing 210023, China

3 Lianyungang Real Estate Registry, Lianyungang 222006, China

Correspondence to: Shuliang Zhang (zhangshuliang@njnu.edu.cn)

Abstract. With rapid urbanization, the scientific assessment of disaster risk caused by flooding events has become an essential task for disaster prevention and mitigation. However, adaptively selecting optimal machine learning (ML) models for flood risk assessment and further conducting spatial and temporal analyses of flood risk characteristics in urban agglomerations remain challenging. This study, establishes a "H–E–V–R" risk assessment index system that integrates hazard, exposure, vulnerability, and resilience based on the factors influencing flood risk in the Yangtze River Delta Urban Agglomeration (YRDUA). Utilizing Automated Machine Learning (AutoML) and the Analytic Hierarchy Process (AHP), a comprehensive flood risk assessment model is constructed. Results indicate that, among those of different assessment models, the accuracy, precision, F1-score, and kappa coefficient of the Categorical Boosting (CatBoost) model for flooded point identification are the highest. Among the flood hazard factors, elevation ranks highest in importance, with a contribution rate of up to 68.55%. The spatial distribution of flood risk in the study area from 1990 to 2020 is heterogeneous, with an overall increasing risk trend. This study is of great significance for advancing disaster prevention, mitigation, and sustainable development in the YRDUA.

1 Introduction

Under global climate change and accelerated urbanization, China has been experiencing pervasive flooding ever more frequently (Tang et al., 2024). Floods threaten people's lives, hinder social development and cause huge economic losses in China (Anon, 2021; Echendu, 2020; Milanesi et al., 2015). Flood formation has been exacerbated by climate change and urbanization, leading to increased frequency, extent, and intensity of urban flooding, and impacting urban flood risk (Mahmoud and Gan, 2018; Khadka et al., 2023; Scott et al., 2023; Seemuangngam and Lin, 2024). Modern human society is faced with the possibility of serious flood hazards and associated challenges, and in addition to post-disaster emergency management, the scientific assessment of disaster risks arising from flood events has gradually become a crucial aspect in preventing and mitigating disasters.

34   Currently, most research in the field of flooding focuses on the flood risks of individual cities (Wang et

35   al., 2021, 2023b; Guan et al., 2024). However, in recent years, the frequency and intensity of urban

36   flooding in China have increased dramatically, and individual cities are no longer able to independently

37   mitigate the risks arising from floods. Studies indicate that China's flood risk management needs to be

38   transformed from the scale of isolated individual cities to the scale of urban agglomerations, conducted

39   in a regionally coordinated manner (Morales-Torres et al., 2016; Wang et al., 2023a). City clusters,

40   constituting the spatial organizational structure of cities that have reached an advanced stage of

41   development, have become key areas for regional disaster management and sustainable development.

42   Due to the unique geographical location and climate conditions of the YRDUA, as well as the impact of

43   urbanization over the past 30 years, the frequency and intensity of flood disasters have been increasing,

44   posing a serious threat to the sustainable development of cities. Therefore, implementing relevant

45   emergency management strategies for flood risks is urgently needed. Furthermore, the region comprises

46   multiple cities, among which distinct resource interactions, such as population mobility and risk transfer,

47   exist (Lu et al., 2022). Thus, it is essential to assess both the overall flood risk characteristics and changes

48   in the urban agglomeration, as well as the spatial correlations of flood risks between cities, explore the

49   mutual influences and interaction mechanisms among regional disaster risks, and provide a scientific

50   basis for sustainable development within the urban agglomeration (Xu et al., 2024).

51   Statistical analyses of historical disaster statistics (Lang et al., 2004), indicator systems methods (Wang

52   et al., 2018b), scenario simulations methods (Yang et al., 2018), and data-driven methods (Abu-Salih et

53   al., 2023), are the primary flood risk assessment method currently. With the development of artificial

54   intelligence technology, data-driven methods, such as machine learning, deep learning, and artificial

55   neural networks, have emerged, providing new opportunities for improving traditional flood risk

56   assessment methods (Liu Jiafu and Zhang Bai, 2015). Ensemble methods are a class of machine learning

57   (ML) techniques that combine multiple base learners to form a stronger predictive model (Webb and

58   Zheng, 2004). They are designed to overcome several limitations of individual models, such as high

59   variance, overfitting, sensitivity to noise, and poor generalization (Yang et al., 2013). By aggregating the

60   outputs of weak learners, ensemble methods significantly enhance model stability, accuracy, and

61   robustness—especially in high-dimensional and complex classification or regression tasks (Kazienko et

62   al., 2015). Various ensemble ML techniques, including bagging (e.g., Random Forest), boosting (e.g.,

XGBoost, CatBoost), and stacking, have been widely used in hydrology, with boosting algorithms in particular showing strong performance in flood prediction and risk assessment (Shafizadeh-Moghadam et al., 2018; Mirzaei et al., 2021; Yan et al., 2024). However, ensemble ML techniques often lack preprocessing and feature selection capabilities, and their application effects vary considerably across different regions. To fully mine data and discover more effective features, experts have proposed other solutions, namely hybrid models such as ANFIS, LSTM-ALO, and LSSVM-GSA (Nayak et al., 2004; Yuan et al., 2018; Adnan et al., 2017). These methods have achieved good performances for given hydrological time series, focusing more on data preprocessing and feature selection. Although research on data-driven urban flood risk assessment methods has increased, certain limitations remain. For example, the physical importance of urban hydrological processes is often ignored in the model assessment process, interpretation of the assessment results is weak, and quantifying the boundaries and scales is challenging (Abu-Salih et al., 2023; Guo et al., 2022).

Furthermore, attempting to combine the data processing and feature selection capabilities of hybrid models with those of integrated models remains challenging (Li et al., 2017). While ML algorithms have demonstrated strong performance in many domains, no single algorithm consistently performs best across all types of problems (Wolpert and Macready, 1997). Therefore, to achieve optimal performance, it is essential to carefully configure key components of the ML pipeline, including feature engineering, model selection, and hyperparameter tuning (Li et al., 2017; Raschka, 2020). Hence, ML applications require the participation of many experts, leading to disproportionate costs for ML development and improvement (Wagenaar et al., 2020; Sarro et al., 2022; Rashidi Shikhteymour et al., 2023). The effectiveness of ML improves with experience, where "experience" refers to the model's iterative exposure to training data and its ability to learn patterns from labeled examples (Jordan and Mitchell, 2015; Nagarajah and Poravi, 2019). One key challenge addressed in this study is how to automatically optimize model components such as feature selection and algorithm configuration in flood risk prediction, while maintaining high accuracy and adaptability across complex hydrological conditions. AutoML is an innovative ML framework that automates key stages of the model development pipeline, including feature selection, model selection, hyperparameter tuning, and ensemble learning (He et al., 2021a). By addressing these challenges, AutoML reduces reliance on expert knowledge and minimizes subjectivity in model building (He et al., 2021b; Consuegra-Ayala et al., 2022). In the context of this study, AutoML

enables the automatic optimization of hazard factor selection, model construction, and parameter

adjustment for flood risk assessment tasks, thereby improving efficiency, objectivity, and reproducibility

in model development. However, AutoML has not been widely applied in the fields of hydrology and

disaster risk management, and research has mainly focused on optimizing the integrated model to achieve

better performance (Özdemir et al., 2023). Continuous research has highlighted the potential role of

AutoML in flood risk detection and assessment (Guo et al., 2022; Vincent et al., 2023; Munim et al.,

2024). Guo et al. (2022) compared AutoML with three single ML algorithms (CatBoost, XGBoost, and

BPDNN) and concluded that AutoML performed better in building rapid warning and comprehensive

analysis models for urban waterlogging. The model based on AutoML can be applied to areas without

water level monitoring and achieve accurate predictions and rapid warnings of waterlogging depth (Guo

et al., 2022; Yan et al., 2024). Abu-Salih et al. (2023) proposed a data-driven flood risk area detection

model that combined the integrated model with the AutoML tool and successfully solved the problems

of data balance and strategy modeling, while reducing the complexity of flood risk area prediction.

Previous studies have provided a theoretical basis and scientific reference for the application of AutoML

methods to flood risk assessment. However, the use of AutoML for research purposes is a complex issue,

and many new opportunities and challenges remain regarding its specific applications.

In the field of flood risk assessment, AutoML has been preliminarily demonstrated to perform well in

flood hazard prediction (Guo et al., 2022c). As an efficient "black-box" modeling approach, AutoML

provides strong support for flood risk modeling through automated feature selection, model training, and

parameter optimization (Hutter et al., 2019; He et al., 2021a). In urban agglomerations, flood risk

assessment is a highly complex task involving diverse natural and socioeconomic factors derived from

heterogeneous and often multi-source datasets (Wang et al., 2023c). These factors—such as rainfall,

topography, land use, drainage, and population density—differ in type and often interact in non-linear

and uncertain ways (Shuster et al., 2005; Zhang et al., 2017; Wang et al., 2018a). Under such complex

circumstances, AutoML struggles to systematically evaluate the multi-dimensional indicators of flood

risk. To address this limitation, this study introduces a multicriteria decision analysis (MCDA) approach

to quantify the importance of various indicators within the evaluation framework (Pham et al., 2021).

MCDA facilitates the integration of such heterogeneous indicators into a unified evaluation framework

by constructing structured weighting schemes, thereby aligning the assessment results more closely with

real-world conditions and expert knowledge (Fernández and Lutz, 2010). In cases where data are limited

122 or certain indicators are difficult to quantify, MCDA methods allow for the incorporation of expert

123 judgment through scoring systems and pairwise comparison matrices, enhancing the practical

124 applicability and robustness of the model (Hites et al., 2006). The analytic hierarchy process (AHP) is

125 one of the most popular MCDA techniques (Donegan et al., 1992). This technique emphasizes the

126 importance of the subjective judgment of decision makers and the consistency of pairwise comparisons

127 of standards in the decision-making process (Saaty, 1980). Recent studies have focused on integrated

128 frameworks of ML models and MCDA technology for flood hazard assessment (Kanani-Sadat et al.,

129 2019; Khosravi et al., 2019; Gudiyangada Nachappa et al., 2020; Mia et al., 2023). However, research

130 focusing on using an integrated framework of AutoML and AHP techniques is still limited.

131 This study develops a flood risk assessment model for the YRDUA by analyzing the factors influencing

132 flood risk and integrating AutoML and AHP methods. In this model, AutoML is employed to construct

133 the flood hazard sub-model, using indicators that represent natural environmental drivers as input

134 features. The hazard is modeled as a binary classification problem (i.e., whether flooding occurs), and

135 the resulting feature importance rankings provide an objective basis for subsequent indicator weighting.

136 Nevertheless, as a data-driven approach, AutoML alone cannot structurally interpret the relative

137 influence of social and systemic factors within a multi-dimensional flood risk assessment framework.

138 Therefore, this study incorporates the AHP to calculate the weights of flood exposure, vulnerability, and

139 resilience in the YRDUA, based on expert knowledge and existing literature. A regional flood risk zoning

140 map is then generated. A comparative analysis with observed inundation points data shows a strong

141 spatial alignment between the distribution of flooded points and the high to medium-high risk zones,

142 highlighting the reliability and applicability of the proposed model. The remainder of this paper is

143 structured as follows: Section 2 describes the study area, data sources, and methodology; Section 3

144 presents the results and analysis; Section 4 discusses the findings and their implications; and Section 5

145 concludes the study with key insights and recommendations.

146 **2 Materials and methods**

147 In this section, the study area is briefly introduced (Section 2.1), and each individual component of the

148 study is further discussed along with the basic geographic information, meteorology, social statistics,

149 historical disaster data, and other fields involved in the study of urban agglomeration flood disasters and

150 their risks (Section 2.2). The framework of the flood risk assessment model is shown in **Figure 1**. The

151 factors influencing flood risk in the YRDUA are explored, and a flood risk assessment index system is

152 established (Section 2.3). The optimal model in AutoML is selected to calculate the importance of flood

153 hazard and hazard characteristic factors (Section 2.4), and the model is combined with AHP to determine

154 the weight of each risk indicator (Section 2.5). Ultimately, a flood risk assessment model based on

155 AutoML and AHP is constructed.
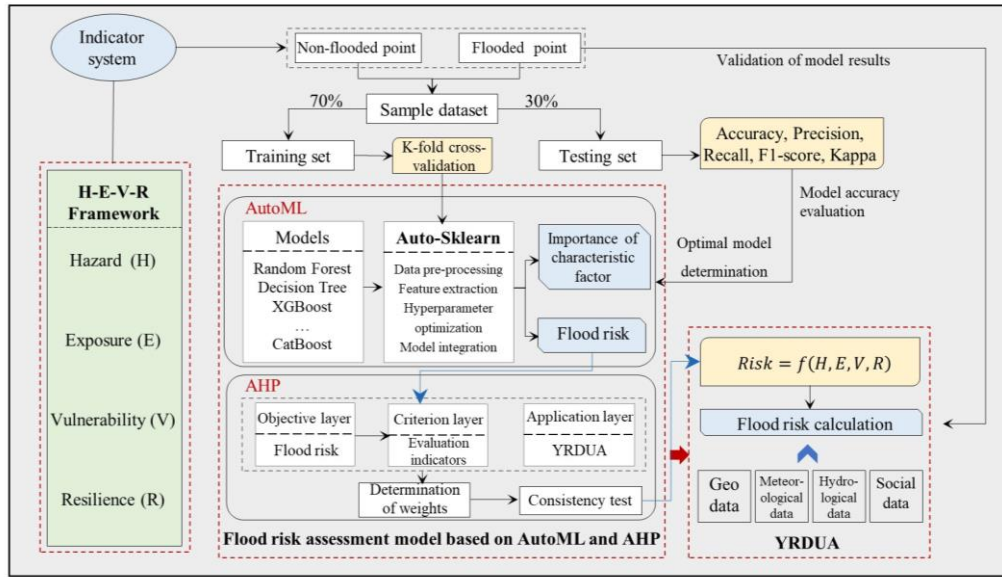
156
157 **Figure 1: Flood risk assessment modeling framework.**
158

159 **2.1 Study area**

160 The Yangtze River Delta Urban Agglomeration, located in the eastern coastal region of China (27° 04′–

161 34° 49′ N; 115° 75′–122° 95′ E), includes 27 cities: 8 in Anhui Province, 9 in Jiangsu Province, 9 in

162 Zhejiang Province, and Shanghai (**Figure 2**) (Yang et al., 2024). Influenced by the East Asian summer

163 monsoon, the study area features low-lying plains in the northern region and higher hilly terrain in the

164 southern region, along with numerous waterways (Ding et al., 2021). With the recent accelerated climate

165 change and urbanization, extreme precipitation events in the Yangtze River Delta (YRD) have been

166 occurring ever more frequently, and the temporal and spatial distribution differences in precipitation have

167 increased. Additionally, the increase in impervious surfaces, narrow plains rivers, and poor drainage may

168 result in more frequent and widespread urban flooding and waterlogging disasters (Wan et al., 2013).

169 This region is economically developed and densely populated , making it the largest urban agglomeration

170 in Asia (Sun et al., 2023). In 2008, the Gross Domestic Product (GDP) of the YRD accounted for 17.5%

171   of the GDP of the entire country, i.e., 4.3 trillion yuan, and the per capita GDP was 44,468 yuan, i.e.,

172   twice the national average level. The population has reached 97.2 million, i.e., 7.3% of China's total

173   population, and the region's average population density is 877 persons/km^2, i.e., approximately twice the

174   national average (Gu et al., 2011). Therefore, the potential risks of flood and waterlogging disasters are

175   substantial.

176
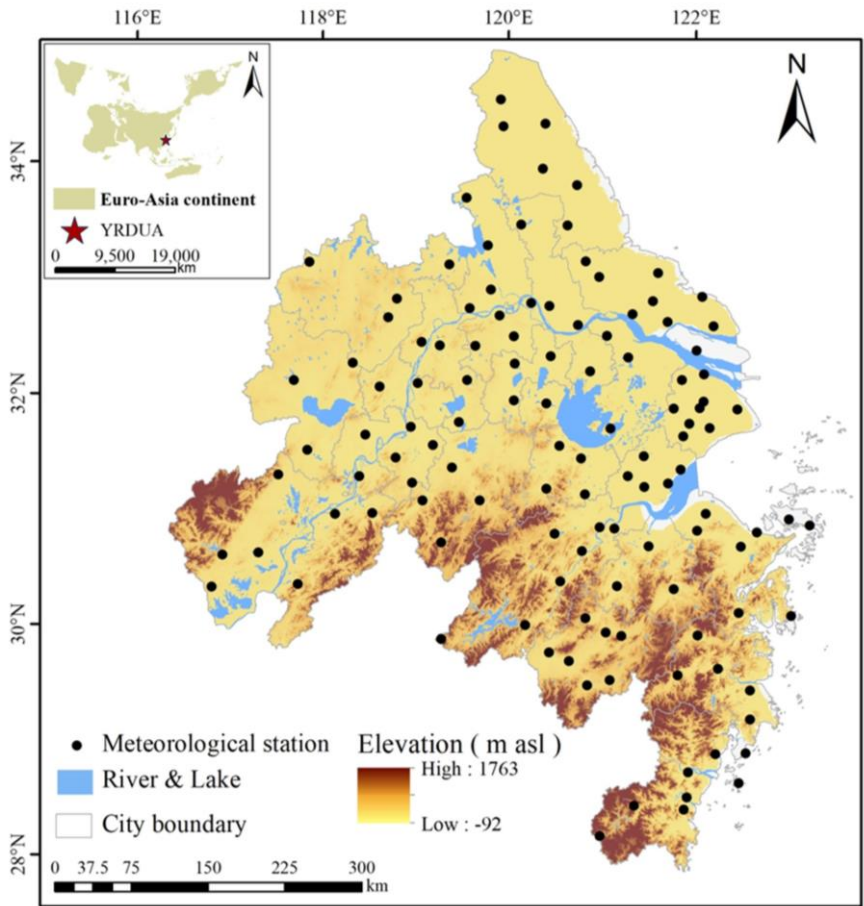
177   **Figure 2: The schematic map of the YRDUA.**

178

179   **2.2 Data sources and Processing**

180   **2.2.1 Data sources**

181   The study of flood disasters and their associated risks in urban agglomerations involves complex natural

182   and socio-economic factors. Therefore, we collected and preprocessed data from multiple fields, such as

183   basic geography, meteorology, social statistics, and historical disasters. **Table 1** lists the data types and

184   resolutions collected for the research area.

185   **Table 1: Description of the Datasets Used for Flood Risk Assessment, Their Characteristics, and Data Sources.**

Category	Details	Resolution	Data Source
Basic Geographic Information Data	Administrative boundaries and river network density data.	30m	-Resources and Environmental Science and Data Center, CAS (https://www.resdc.cn/). -USGS (https://earthexplorer.usgs.gov/). -Wuhan University CLCD dataset (https://zenodo.org/records/8176941). - National Ecosystem Science Data Center (nesdc.org.cn).
	Digital Elevation Model (DEM) based on SRTM1 (30m), mosaicked and clipped to the study area (27 core cities).		
	Land use data from CLCD (30m), includes 7 types: farmland, forest, shrubland, grassland, water, bare land, and impervious surfaces.		
	NDVI data (2000–2020) calculated using the GEE platform.		
Meteorological Data	Hourly precipitation data from 120 meteorological stations. Data preprocessed for outlier removal and missing value handling.	Station data	National Meteorological Information Center, China Meteorological Administration
Social Statistics	Population, unemployment, GDP, and healthcare statistics at the prefecture level.	Prefecture-level	Provincial and municipal statistical yearbooks and bulletins
	Urbanization rate calculated using urban population proportion.		
	GDP density and per capita GDP derived from total GDP and land area/population.		
Historical Disaster Data	Flood inundation data from the MODIS-based Global Flood Database (2000–2018), processed to focus on the YRDUA region. To ensure comprehensive selection of inundation points, the inundated areas within the time frame were overlaid to produce a historical flood map.	250m	Global Flood Database (https://www.emdat.be/).

186

187 **2.2.2 Data Standardization and Preprocessing**

188 Due to variations in data sources and formats, the collected flood disaster risk data exhibit differences in

189 spatial resolution, dimensions, and magnitude. To ensure consistency and comparability, standardization

190 of both spatial scale and numerical range was performed before using these datasets as flood risk

191 indicators.

192 (1) Unification of spatial scale means aligning data within the same coordinate range and resolution. The

193 research data is standardized through projection transformation, converting all datasets into the same

194 geographic and projected coordinate systems. To generate continuous spatial surfaces from discrete data

195 points, we applied the Ordinary Kriging interpolation method, which assumes a constant but unknown

196 local mean (Cressie, 1990). A spherical semivariogram model was adopted to capture spatial

197 autocorrelation, as it is widely used in environmental geostatistics for its bounded range and smooth

198 continuity (Webster and Oliver, 2007). The interpolation process was carried out using ArcGIS 10.8.

199 Finally, if the spatial data has different resolutions, resampling is performed to standardize all data to the

200 same resolution, which in this study is unified to 30m×30m.

201 (2) Normalization of the numerical range can be achieved using a normalization process. In this study,

202 the Min-Max normalization method is applied. Specifically, the minimum and maximum values of each

203 feature are computed only from the training set, and both the training and test sets are then normalized

204 using these training-derived parameters. This ensures that the normalized values in the training set are

205 scaled to the range [0,1], while the values in the test set may exceed this range if they fall outside the

206 training set's value distribution. The formula is as follows:

207 $$x' = \frac{x - x_{min}^{train}}{x_{max}^{train} - x_{min}^{train}} \tag{1}$$

208 **2.3 Historical Flood Inundation Point Extraction**

209 The historical flood inundation map of the study area is shown in **Figure 3** (a). The flood inventory map

210 used in this study was created based on inundation data from the Global Flood Database and the EM-

211 DAT flood disaster database, and further verified through satellite imagery, Google Earth, and

212 documented historical flood records. The actual flooded areas were delineated from flood traces in the

213 inundation dataset and image interpretation. A flooded point is defined as a location that lies within the

214 inundation extent of at least one recorded flood event during the study period. Based on this definition,

278 flooded points were randomly selected from the validated inundated areas. These points serve as the

foundation for subsequent statistical analysis and model training, with their spatial distribution shown in

Figure 3 (b).

To calculate flood hazard, it is necessary to select training samples. The task of identifying flooded and

non-flooded points using AutoML is essentially a binary classification problem, which requires a

balanced number of samples. An imbalanced ratio of positive and negative samples can result in

unreliable classification outcomes. Previous studies (Pham et al., 2021; Bostan et al., 2012) have shown

that the best classification performance is achieved when the ratio of flooded to non-flooded points is

1:1. Therefore, after selecting the flooded points, 278 non-flooded points were randomly sampled to

ensure a balanced 1:1 ratio, excluding high-altitude areas, based on the region's actual characteristics.

Finally, the flooded and non-flooded points were used as sample data and divided into a 7:3 ratio (70%

for training and 30% for testing) for model training.
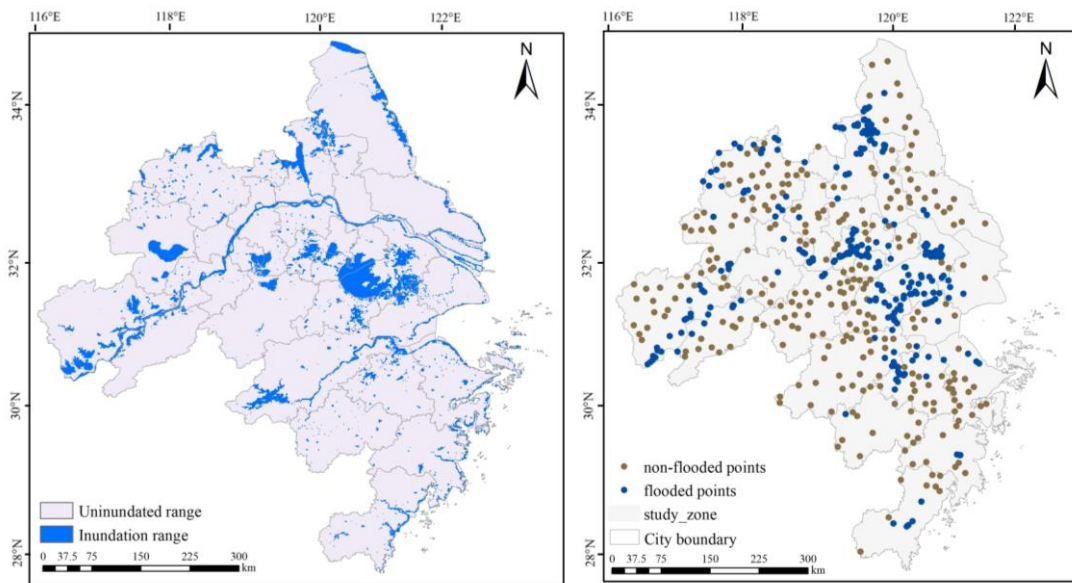
Figure 3: (a) Flood inundation map of the study area. (b) Spatial Distribution of Flooded and Non-Flooded Points in the YRDUA.

2.4 Establishment of an flood risk assessment indicator system

Although risk is a universal concept, it has no universal definition (Aven, 2016; Mishra and Sinha, 2020).

Based on the hazard–exposure–vulnerability (H–E–V) disaster risk framework, we considered the

particularity of flood risk research at the urban agglomeration scale, incorporated resilience indicators

into the existing framework, and constructed a four-dimensional flood risk assessment framework of hazard–exposure–vulnerability–resilience (H–E–V–R) that can assess regional flood risks more comprehensively and systematically. The conceptual description of flood risk in this study can be expressed in the Eq. (2):

$$Risk = f(H, E, V, R) = \sum_{i=1}^{a} \omega_H H_i + \sum_{i=1}^{b} \omega_E E_i + \sum_{i=1}^{c} \omega_V V_i + \sum_{i=1}^{d} \omega_R R_i, \qquad (2)$$

where H, E, V, and R represent the danger of, exposure to, vulnerability to, and resilience in response to floods, respectively; ω_H, ω_E, ω_V, and ω_R are the weights of danger, exposure, vulnerability, and resilience, respectively; H_i, E_i, V_i, and R_i are the values of items i of the indicators, respectively; and a, b, c, and d are the numbers of the indicators, respectively.

We constructed a flood risk assessment index system for the YRDUA based on the "H–E–V–R" framework, the actual situation of the study area, the formation mechanisms of flood disasters, and the findings of relevant studies (Gain et al., 2015; Criado et al., 2019; Hsiao et al., 2021). We selected four first-level indicators (i.e., hazard, exposure, vulnerability, and resilience indices) and 19 second-level indicators. A detailed description of the flood risk assessment index system is presented in 错误!未找到引用源。.
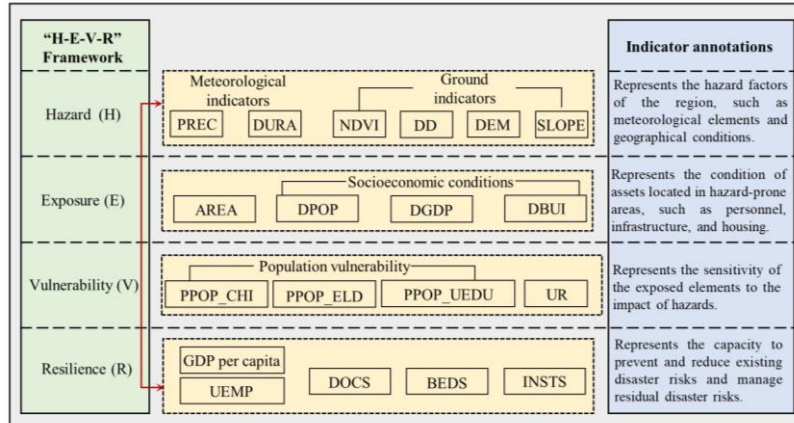
Figure 4: Flood risk assessment index system for the YRDUA based on the H–E–V–R framework.

The hazard indicators consisted of six indices: Average annual precipitation (PREC), Annual Cumulative Heavy Rainfall Duration (DURA), Digital Elevation Model (DEM), SLOPE, Drainage Density (DD), and Normalized Difference Vegetation Index (NDVI). Rainfall is the primary factor leading to flooding, particularly extreme rainstorms caused by climate change. According to the Meteorological Bureau's

256 definition, a heavy rainstorm event is characterized by rainfall of 50mm or more within 24 hours. DURA

257 is defined as the total number of days with heavy rainstorm events occurring at all meteorological stations

258 within the study area each year. The more days heavy rainstorms accumulate and the longer their duration,

259 the greater the likelihood of flooding and other disaster events. DEM and SLOPE are important

260 topographical indicators. Areas with low DEM and SLOPE values are generally more susceptible to

261 flood threats. DD refers to the area of rivers or lakes per unit of land surface area and is a crucial indicator

262 of a watershed's structural characteristics. It determines the watershed's capacity to withstand flooding.

263 The higher the DD, the greater the likelihood of flooding and the higher the potential flood risk.

264 Vegetation plays a role in water storage, retention, and infiltration. The lower the vegetation coverage,

265 the weaker the buffering capacity, making it more likely for surface water to accumulate. The NDVI

266 index measures the relative abundance of green vegetation, with values ranging from -1 to 1. The higher

267 the value, the greater the vegetation coverage, and the lower the risk of flooding.

268 Land area (AREA), Population Density (DPOP), GDP Density (DGDP), and Building Density (DBUI)

269 were selected as exposure indicators to assess the degree of vulnerability of both the natural environment

270 and social systems to flooding. The land area for each administrative unit at the prefecture-level city is

271 calculated individually. A larger land area corresponds to a greater extent exposed to flooding. DPOP

272 and DGDP represent the concentration of population and assets, respectively. Areas with higher DPOP

273 and DGDP are more susceptible to potential threats from pluvial flooding. DBUI, the ratio of total

274 building area to total land area in a region, indicates the building density. A higher DBUI reflects greater

275 exposure to flooding.

276 Vulnerability indicators focus more on the social aspects of flood disasters. This study selects four

277 vulnerability indicators: Proportion of Child Population (PPOP_CHI), Proportion of Elderly Population

278 (PPOP_ELD), Proportion of Uneducated Population (PPOP_UEDU), and Urbanization Rate (UR). Age

279 is a key feature of social vulnerability, and both the population aged 0-14 and those over 65 are considered

280 vulnerable groups, as these age groups are more susceptible to flood damage. The uneducated population

281 generally has a weaker awareness of disaster risks and lower self-protection capacity, which makes this

282 group more vulnerable to flooding. The urbanization rate refers to the proportion of the urban population

283 in the total resident population of a region. This indicator is inversely related to flood vulnerability. In

284 general, a higher urbanization rate indicates greater social development and stronger protective capacities,

285 which can reduce vulnerability to flooding to some extent.

286   The resilience indicators selected in this study include Gross Domestic Product (GDP) per capita,

287   Unemployment Rate (UEMP), Number of Doctors (DOCS), Number of Medical Institutions (INSTS),

288   and Number of Hospital Beds (BEDS). GDP per capita is the ratio of a region's GDP to its total resident

289   population over a specified period, reflecting the region's economic condition. A higher GDP per capita

290   indicates a more developed economy, which is associated with a greater capacity to recover quickly after

291   a flooding event. The Unemployment Rate (UEMP) measures the proportion of the idle labor force,

292   indirectly reflecting the stability of urban development. A high unemployment rate signals economic

293   instability, which weakens the capacity to cope with floods and extends the time required for post-disaster

294   recovery, thus impeding disaster response efforts. The indicators of DOCS, INSTS, and BEDS provide

295   insights into a region's healthcare and medical support capabilities. Areas with stronger healthcare

296   systems are better positioned to manage flood risks and recover more effectively from such disasters.

297

2.5 Flood risk calculation method based on AutoML

2.5.1 Feature selection

300   The flood inventory map in this paper was developed using inundation data from the Global Flood

301   Database and flood disaster data from the EM-DAT database, supplemented by satellite and Google

302   image interpretation and verified against existing historical flood records. The actual flood-affected areas

303   were delineated based on flood traces from the inundation datasets and image interpretations. For this

304   study, 278 flood inundation points were randomly selected within the inundation data range during the

305   study period, and the location of each point was used as the basis for subsequent statistical analysis of

306   flood events. The main factors affecting flood risk were considered during input feature selection.

307   Rainfall and rainstorms are important factors that lead to floods, and flooding is closely related to

308   topography, slope, vegetation cover, and hydrological conditions. Therefore, six indicator factors,

309   namely PREC, DURA, DEM, SLOPE, NDVI, and DD, were selected as the input features of the model.

310   To verify the model, 70% of the data in the sample were set as the training dataset and the remaining 30%

311   of the data were set as the testing dataset through random sampling.

312   When the number of samples is small, data balancing is essential to ensure uniform sampling and reduce

313   the deviations among the training, validation, and original datasets. Data balancing refers to the process

314   of achieving a balanced distribution of data for each labeled category; it is particularly important when

315   the number of observations in each class is significantly different. One way to address an imbalanced

316   dataset is to oversample the minority classes. In this study, we assessed flood risk based on the

317   identification of flooded point in the sample, which is essentially a binary classification problem;

318   therefore, the output features are 0, i.e., negative categories (non-flooded points), versus 1, i.e., positive

319   categories (flooded points). The processed dataset comprised 278 positive samples (flooded points) and

320   278 negative samples (non-flooded points), with each label consisting of 278 points representing the

321   entire dataset.

322   **2.5.2 Model training and hyperparameter optimization**

323   Training samples were generated using the data from flooded and non-flooded points in the study area,

324   and the Auto-Sklearn was used for model training, its principle is shown in **Figure 5**. The Auto-sklearn

325   framework has multiple built-in machine learning algorithms. We selected 9 models that are more typical

326   or have better performance in flood hazard research: random forest (RF), extreme gradient boosting

327   (XGBoost), Light Gradient Boosting Machine (LightGBM), categorical feature boosting (CatBoost),

328   Extra trees, Decision tree, Nearest Neighbors, Multi-layer Perceptron (MLP) neural network, and Linear

329   Regression. The training and testing datasets were used to train the 9 machine learning models, and the

330   hyperparameters were continuously adjusted and optimized.

331
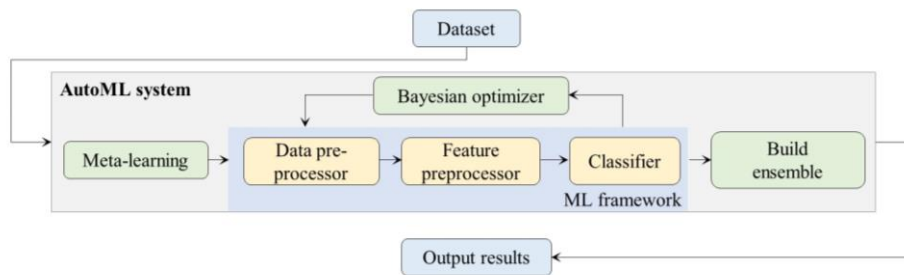
332   **Figure 5: Principles of Auto-Sklearn**

333

334   Hyperparameter optimization is an important step in ML model training. The aim of this step is to

335   determine a hyperparameter combination to generate a ML model that performs well on a specific dataset

336   and reduces the effect of the predefined loss function on a given dataset. In this study, we used a grid

337   search strategy for optimization. For each set of hyperparameter combinations, k-fold cross-validation

338   was used to evaluate the model. To quantify the balance between Precision and Recall, the F1-score was

339   used as the primary evaluation metric. The hyperparameter combination corresponding to the model with

340 the highest average F1-score was selected as optimal. Briefly, the training dataset was divided into K

341 parts, of which one was selected as the test set and the rest were used as the training set. The cross-

342 validation was repeated K times and the results were averaged K times. The model with the best average

343 result among all models was selected as the optimal model, and the final classification prediction result

344 was the output. In this study, we used 5-fold cross-validation.

345 It is important to note that 5-fold cross-validation was employed at two distinct stages in this study. First,

346 it was conducted within the training set during hyperparameter tuning as part of the AutoML model

347 selection process. Second, following final model selection, an independent 5-fold cross-validation was

348 applied to the entire dataset to evaluate the generalization performance of the model and identify potential

349 overfitting. The data partitions used in the two stages were entirely separate, ensuring that no data leakage

350 occurred.

351 **2.5.3 Performance evaluation**

352 To better compare the performance of the 9 selected ML models in the Auto-Sklearn framework for flood

353 risk assessment, multiple evaluation indicators were used to assess the test dataset. The following

354 combinations of the true category of the sample point and the category predicted by the classifier were

355 used: True Positive (TP)—the sample point is a flooded point, and the model classifier also predicts that

356 it is a flooded point; True Negative (TN)—the sample point is a non-flooded point, and the model

357 classifier also predicts that it is a non-flooded point; False Positive (FP)—the sample point is a non-

358 flooded point, and the model classifier mistakenly predicts that it is a flooded point; False Negative

359 (FN)—the sample point is a flooded point, and the model classifier mistakenly predicts that it is a non-

360 flooded point. Therefore, four related indicators were selected: Precision, Recall and F1-score, and the

361 consistency metric Kappa coefficient. The calculation formulas are as follows:

362 $$Precision = \frac{TP}{TP+FP} \ , \tag{3}$$

363 $$Recall = \frac{TP}{TP+FN} \ , \tag{4}$$

364 $$F1-_{score} = \frac{2TP}{2TP+FP+FN} \ , \tag{5}$$

365 Among the indicators, *Precision* refers to the proportion of correctly predicted flooded points among all

366 predicted flooded points, reflecting the model's ability to avoid false positives. *Recall* measures the

367 proportion of correctly identified flooded points among all actual flooded points, representing the

368 model's sensitivity. *F1-score* is the harmonic mean of Precision and Recall, providing a balanced

369 evaluation of both metrics and reflecting the overall recognition performance of the model.

370 *Kappa* coefficient is a statistical consistency metric used to measure classification performance, which

371 is calculated based on the confusion matrix of true and predicted categories. Its value ranges from [-1,1]:

372 A Kappa value of 1 indicates perfect agreement, 0 means the classification is no better than random

373 guessing, and negative values suggest the classification is worse than random prediction. *Kappa* is

374 calculated using Eq. (6), where P_e is given by Eq. (7).

375 $$Kappa = \frac{P_o - P_e}{1 - P_e},$$ (6)

376 $$P_e = \frac{(TP+FP)(TP+FN)+(TN+FN)(TN+FP)}{(TP+FP+TN+FN)^2},$$ (7)

377 where P_e represents the expected agreement by chance.

378 Combining multiple indicators allows for a more comprehensive evaluation of models within the Auto-

379 Sklearn framework for flood point identification and flood risk assessment.

380 **2.6 Method for determining flood risk index weights based on AHP**

381 **2.6.1 Establishing a hierarchical model**

382 According to the decision-making objectives, factors, and applications in decision-making problems, the

383 AHP can be divided from bottom to top into the target, criterion, and application layers. Among them,

384 the target layer is the problem to be solved (i.e., final flood risk). The criterion layer is the intermediate

385 link, including the factors to be considered and the decision making criteria. The factors can be divided

386 into different evaluation indicators, including four first-level indicators (danger, exposure, vulnerability,

387 and resilience) and their corresponding 19 second-level indicators. The criterion layer comprises various

388 weight combination schemes linked to the target layer. The application layer is the final optional scheme

389 and specific application of the decision. The final weight scheme and evaluation results of this study

390 were applied to the YRDUA.

2.6.2 Constructing the judgment matrix

After the hierarchical structure was established, a judgment matrix was constructed based on the relationship between the criteria and indicators. Different elements in the sublevel were compared pairwise, and the relative importances of all elements in the current layer and previous layer were compared. Typically, a pairwise comparison matrix is used as representative. In this study, we adopted the 1–9 scale method as the importance measurement standard. The importance comparison relationship is presented in **Table 2**, where the matrix element a_{ij} represents the comparison result of the ith element relative to the jth element.

Table 2: Pairwise comparison point-based rating scale of AHP.

Ranking	Importance Level
1	Equally important
3	i is slightly more important than j
5	i is much more important than j
7	i is very much more important than j
9	i is extremely important than j
2, 4, 6, 8	Intermediate value of two adjacent judgments
Reciprocal	Comparative judgment of j vs., $a_{ji} = 1/a_{ij}$

2.6.3 Solving the eigenvector of the judgment matrix

Based on the judgment matrix, the square root method was used to solve the eigenvector and eigenroot. The first step is to calculate the square root a_{ij} of the product of each row of the judgment matrix n, then normalize it, and finally calculate the maximum eigenroot of the judgment matrix. The formula is as Eq. (8), Eq. (9), Eq. (10).

$$M_i = \sqrt[n]{\prod_{j=1}^{n} a_{ij}}, \tag{8}$$

$$W_i = \frac{M_i}{\sum_{i=1}^{n} M_i}, \tag{9}$$

$$\lambda_{max} = \sum_{i=1}^{n} \frac{(AW)_i}{nW_i}, \tag{10}$$

2.6.4 Consistency check

After the eigenvector calculation is completed, a consistency test is required to reduce the subjectivity in the judgment matrix and enhance the scientific nature of the data and calculations. In a pairwise comparison matrix, consistency means that the decision-maker's judgments must exhibit logical coherence and transitivity. Specifically, if option A is considered more important than option B, and option B is considered more important than option C, then consistency requires that option A must also be judged more important than option C (Saaty, 1984).

The consistency indicator (CI) is used to measure the deviation of the judgment matrix from the consistency: the smaller the CI, the greater the consistency of the judgment matrix. When CI = 0, the judgment matrix is completely consistent. The CI calculation formula is as Eq. (11).

$$CI = \frac{\lambda_{max}-n}{n-1},$$
(11)

To quantify the standard, the relative consistency (CR) index was further calculated as Eq. (12).

$$CR = \frac{CI}{RI},$$
(12)

Where average Random Consistency Index (RI) represents the average random consistency which depends only on the order of the judgment matrix. The RI values for judgment matrices of order 1 to 10 are shown in **Table 3**.

Table 3: Consistency index (RI) for a randomly generated matrix.

n	1	2	3	4	5	6	7	8	9	10
RI	0.00	0.00	0.52	0.89	1.12	1.26	1.36	1.41	1.46	1.49

CR was determined based on the RI value. When CR < 0.1, the consistency of the judgment matrix is considered good. When CR > 0.1, the consistency of the judgment matrix is unacceptable, and the judgment matrix must be adjusted and modified. In such cases, the corresponding judgment matrix was further constructed, and the eigenvector and eigenroot were calculated using the following formulas:

Finally, the judgment matrix that passed the consistency test was used to calculate the weights of the indicators at the different levels.

2.7 Determination of flood risk levels

The classification of flood risk levels often involves manually setting thresholds, which can introduce subjectivity and influence the accuracy of the risk assessment outcomes (Ma et al., 2022). To calculate the flood risk, we employed the natural breakpoint classification method, which groups data into classes based on natural divisions within the dataset (Lin et al., 2019). This method works by identifying points where the data distribution changes most significantly and dividing the data into ranges based on these breaks. Unlike clustering methods, which do not focus on the number and range of elements in each group, the natural breakpoint method ensures that the range and number of elements in each group are as balanced as possible (Ma et al., 2022).

3 Results and discussion

3.1 Model flood risk results and evaluation

3.1.1 AutoML optimal model selection

In the experiment, 9 typical ML models under the Auto-Sklearn framework were used to process the sample dataset, with 70% of the sample set being used as the training dataset and 30% being used as the testing dataset. The results of the comparative analysis of the model performance based on the test dataset are presented in **Table 4**. A comprehensive analysis of the results on the testing data revealed that, in terms of Precision, CatBoost had the highest value (0.9030), followed by LightGBM (0.8960) and Extra Trees (0.8893). Meanwhile, CatBoost had the highest recall rate of 0.8883, followed by that of Extra Trees at 0.8870. The probability thresholds for Precision, Recall, and F1-score range from [0,1], while the Kappa coefficient ranges from [-1,1]. The F1-score and Kappa coefficient of the CatBoost model were also markedly higher than those of the other models, reflecting the model's good consistency. A comprehensive comparison showed that the precision, F1-score, and Kappa coefficient of the CatBoost model were the highest, with its precision reaching 0.9030, indicating that the recognition and prediction precision of the flooded points in the study area based on the CatBoost model were obviously better than those of other common machine learning models.

Since flood data often involve various environmental factors and complex interactions, the CatBoost model is highly effective at handling these nonlinear relationships and feature interactions. Additionally, the model incorporates multiple regularization mechanisms during tree construction, which helps reduce

461 overfitting and enhances the model's generalization capability. As shown in **Table 4**, most models

462 performed well on the training set, but their performance slightly declined on the test set, highlighting

463 variations in generalization ability. CatBoost demonstrated strong robustness, achieving a Precision of

464 0.9319 on the training set and 0.9030 on the test set. Additionally, LightGBM and XGBoost showed

465 relatively consistent performance between the training and test sets, suggesting better generalization.

466 However, models such as Decision Tree and Nearest Neighbors exhibited a more significant performance

467 drop in the test set, indicating a higher sensitivity to overfitting. Interestingly, in a few cases (e.g., Extra

468 Trees), test set performance slightly exceeded that of the training set in certain metrics. This is not

469 uncommon in small, balanced datasets and may result from a combination of factors such as random

470 sampling variation, slightly easier test samples, or appropriate regularization that reduces overfitting in

471 the training set. To further evaluate overfitting, we used 5-fold cross-validation by comparing the

472 performance of the training and testing sets. The experimental results indicate that while most models

473 showed some performance decline on the test set, CatBoost maintained relatively stable performance,

474 suggesting that the model does not exhibit significant overfitting and has good generalization ability.

475 **Table 4: Comparative analysis of the performances of different ML models.**

Models	Dataset	Precision	Recall	F1-score	Kappa
CatBoost	Training set	0.9319	0.9307	0.9547	0.8614
	Testing set	0.9030	0.8883	0.8960	0.7915
XGBoost	Training set	0.9017	0.8827	0.8818	0.8640
	Testing set	0.8748	0.8640	0.8624	0.7256
LightGBM	Training set	0.9349	0.9307	0.9306	0.8616
	Testing set	0.8960	0.7890	0.8015	0.7324
Random Forest	Training set	0.8922	0.8747	0.8745	0.7484
	Testing set	0.8482	0.8320	0.8309	0.6662
Extra Trees	Training set	0.8524	0.8240	0.8735	0.7695
	Testing set	0.8893	0.8570	0.8877	0.7751
Decision Tree	Training set	0.8886	0.8640	0.8621	0.8040
	Testing set	0.8810	0.8720	0.8708	0.7419
Linear Regression	Training set	0.8636	0.8533	0.8525	0.7073
	Testing set	0.8682	0.8480	0.8450	0.6926
Nearest Neighbors	Training set	0.7301	0.7907	0.7987	0.6009
	Testing set	0.7747	0.7440	0.7390	0.4937

Models	Dataset	Precision	Recall	F1-score	Kappa
MLP Neural Network	Training set	0.8998	0.8880	0.8873	0.7765
	Testing set	0.8682	0.8480	0.8450	0.6926

476

By comparing the performances of the 9 models, we found that the CatBoost model was more effective in identifying flooded points. To further verify the excellent performance of the model, the receiver operating characteristic (ROC) curve and area enclosed by the coordinate axes (corresponding area under the curve [AUC] value) were plotted based on the test dataset to assess the model's binary classification effectiveness: the larger the AUC value, the better the model distinguishes between classes. When AUC > 0.8, the model prediction effect is very good (Sinha et al., 2008). In this study, both micro- and macro-average ROC curves were plotted. The micro-average ROC curve aggregates the contributions of all classes to compute the average ROC curve, treating each instance equally, while the macro-average ROC curve computes the ROC curve for each class independently and then averages the results. These two methods are commonly used for multi-class classification problems, but in this study, they were used to give a more comprehensive comparison of model performance. The verification results are shown in **Figure 6**. The AUC value of the CatBoost model reached 0.91, guaranteeing the performance and prediction reliability of the CatBoost model. Based on this, the CatBoost model was selected to calculate the flood risk in the YRDUA.
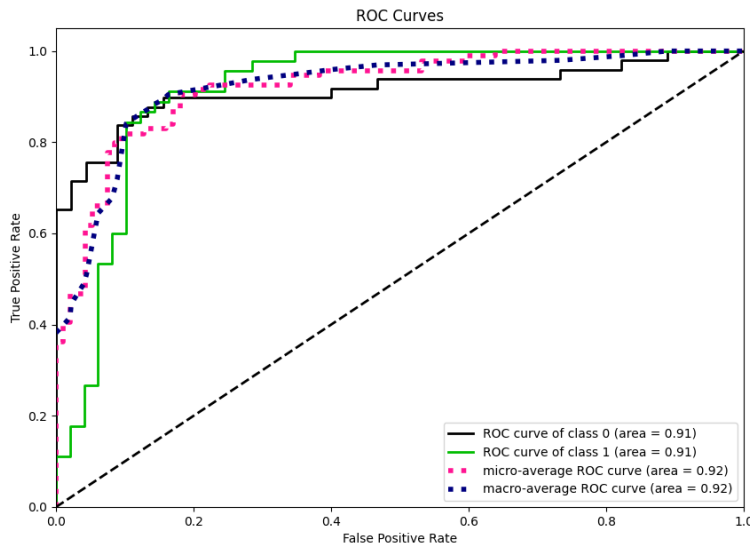
Figure 6: Receiver operating characteristic (ROC) curves and corresponding area under the curve (AUC) values of the CatBoost model.

3.1.2 Importance and Interpretability Analysis of Hazard Factors

In this study, the AutoML model was used specifically to assess flood hazard, which represents the physical likelihood of flood occurrence and is directly driven by environmental factors such as rainfall, topography, and drainage characteristics. Therefore, only the six second-level indicators under the hazard dimension were used as input features in the AutoML model. This approach allowed us to focus the model on identifying the key natural drivers of flooding, while the other dimensions — exposure, vulnerability, and resilience—were later incorporated via the AHP method for comprehensive flood risk evaluation.

To better understand the contribution of different hazard indicators to flood risk in the YRDUA, we conducted both importance ranking analysis using the CatBoost model and interpretability analysis based on SHAP.

The CatBoost model was used to quantify the relative importance of six key hazard indicators. The results, shown in **Figure 7**, reveal significant differences in their influence. DEM was identified as the most critical factor, contributing 68.55%, which far exceeds the other factors, which is also in line with the findings of many researchers within the region (Mei et al., 2021; Wan et al., 2013). Low-lying areas naturally function as water accumulation zones, increasing flood vulnerability. Additionally, urban areas in the YRDUA are dominated by impervious surfaces, limiting infiltration and exacerbating flood risks. While PREC is a primary factor in storm-induced flooding, its direct contribution to flood risk was relatively low compared to DURA, which accounted for 10.07%. This highlights that the persistence of extreme rainfall events is a stronger predictor of flood hazard than total annual precipitation.

515
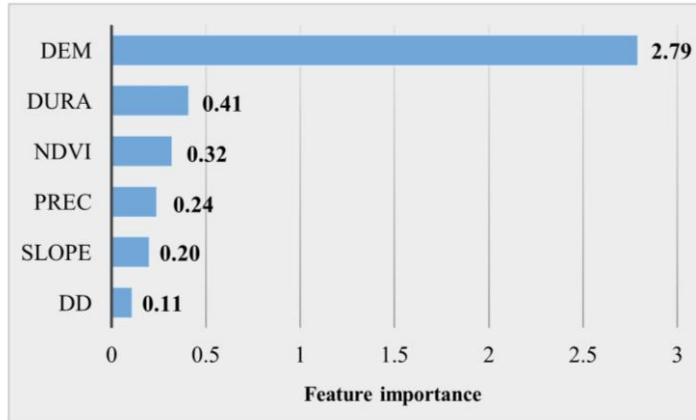
516 **Figure 7: Importance Ranking of Hazard Factors Based on the CatBoost Model**

517

518 To further analyze the interpretability of the model and understand the impact of individual flood hazard

519 indicators on the model's classification results, this paper calculates Shapley Additive Explanations

520 (SHAP) to indicate the contribution of each feature in the sample (Lundberg and Lee, 2017). SHAP, a

521 game theory-based post-hoc interpretation method, quantifies the marginal impact of each feature on

522 model predictions. The SHAP summary plot in **Figure 8** (a) ranks features based on their absolute SHAP

523 values, consistent with the CatBoost importance ranking. Each row represents a feature, where red

524 indicates higher feature values and blue indicates lower values. The results show that DEM, SLOPE, and

525 NDVI negatively impact flood risk, meaning that higher elevation, steeper slopes, and greater vegetation

526 coverage reduce flood hazards. In contrast, DD, DURA, and PREC positively impact flood risk,

527 indicating that higher drainage density, longer durations of extreme rainfall, and increased precipitation

528 levels contribute to higher flood hazards. Among these, DEM has the highest absolute SHAP value, with

529 a strong clustering below zero, reinforcing its dominant role in flood risk determination.

530
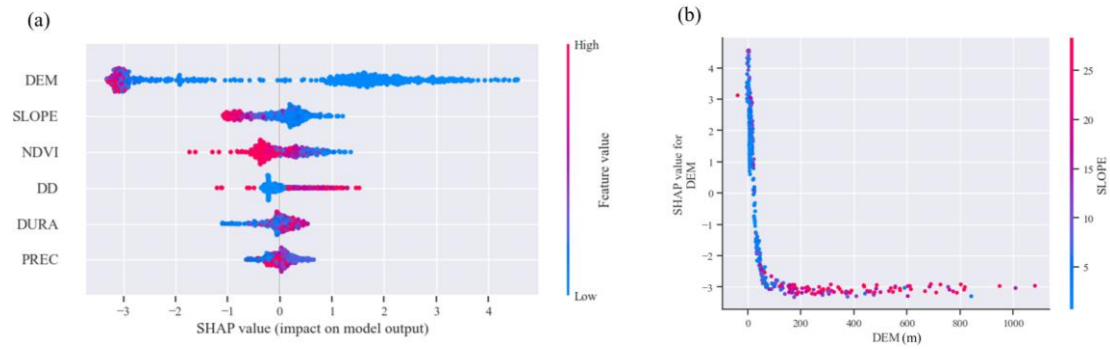
Figure 8: (a) Scatter Plot of Hazard Indicators from SHAP Analysis. (b) SHAP Dual Dependence Analysis of

532 **Elevation and Slope Factors.**

533

534 To directly capture the interaction effects between paired indicator factors, this study used SHAP

535 interaction values based on game theory, ensuring consistency while also explaining the interaction

536 effects of individual predictions. For the DEM feature, which had the highest importance in the SHAP

537 analysis, the factor most strongly correlated with it was SLOPE. Therefore, to illustrate how one feature

538 interacts with another to affect the model training results, this study used DEM and SLOPE as examples

539 to plot the SHAP interaction scatter plot, representing the dependency of the DEM feature. The results

540 are shown in **Figure 8** (b). This dependency plot takes the form of a logarithmic function, indicating that

541 as DEM increases, the flood hazard decreases. Additionally, the slope has a negative effect on the flood

542 hazard in relation to elevation; that is, at lower elevations and gentler slopes, the flood hazard is greater.

543 **3.1.3 Determination of flood risk index weights**

544 A judgment matrix was constructed for 19 indicator factors. A hazard index was constructed based on

545 feature importance calculated using AutoML. The exposure, vulnerability, and resilience indicators were

546 determined based on existing literature and relevant expert scores (Hsiao et al., 2021). The judgment

547 matrices were constructed using a hybrid approach. For the hazard indicators, feature importance scores

548 generated from the AutoML model were used to inform the pairwise comparisons. For the exposure,

549 vulnerability, and resilience indicators, the weights were determined by the authors based on a

550 combination of expert judgments, a review of existing studies, and consideration of the local conditions

in the YRDUA. The Saaty 1–9 scale was applied to assign relative importance to each pair of indicators. Finally, the judgment matrix results were tested for consistency, and the CR value was 0.0058, i.e., << 0.100, indicating that the results passed the consistency test and that the flood risk index weight values calculated using the AHP were acceptable. The specific indicator weights and their corresponding impacts on flood risk are shown in Table 5. The "Attribute" column represents the impact of each indicator on flood risk, with "+" indicating a positive impact on flood risk and "-" indicating a negative impact on flood risk.

Table 5: Flood risk index weights.

Dimension	Indicator	Unit	Attribute	Weight
Hazard (0.4798)	PREC	mm	+	4%
	DURA	Day	+	10.8%
	NDVI		-	7.6%
	DEM	km	-	22.99%
	SLOPE	°	-	6.4%
	DD	km/km^2	+	3.2%
	AREA	km^2	+	1.1%
Exposure (0.1083)	DPOP	people/km²	+	4.32%
	DGDP	10,000 yuan/km²	+	3.84%
	DBUI	km^2	+	1.16%
Vulnerability (0.1312)	PPOP_CHI	%	+	4.92%
	PPOP_ELD	%	+	3.04%
	PPOP_UEDU	%	+	2.11%
	UR	%	-	2.05%
Resilience (0.2807)	GDP per capita	100 million yuan/10,000 People	-	4.43%
	UEMP	%	+	5.04%
	DOCS	Per person	-	4.13%
	INSTS	Each	-	0.45%
	BEDS	Per bed	-	6.28%

560 The weighted results reflect the degrees of influence of the different indicator factors on flood risk.

561 Danger was the decisive factor affecting flood risk, with a weight of 0.4798, followed by resilience and

562 vulnerability. Exposure had a relatively low impact on flood risk. In terms of danger, the topography and

563 DURA were the main factors affecting the occurrence of flooding. These two indicators determined the

564 characteristics of flood disasters in the YRDUA from the perspective of disaster-prone environments and

565 driving factors, respectively. In terms of exposure, the YRDUA is a typical area with rapid social,

566 economic, and population growths in China. High population and GDP densities increase the risk of

567 flood exposure. In addition, the uneven age distribution and education levels of the population are

568 important social factors affecting the risk of flood disasters in urban agglomerations. In terms of

569 resilience, improving health and medical infrastructure, developing the regional economy, and reducing

570 unemployment rates are conducive to improving the overall disaster response capacity of the region and

571 reducing the risk of flood disasters in the YRDUA.

572 **3.1.4 Model results verification**

573 Based on CatBoost under the AutoML framework and AHP, the levels of flood hazard, exposure,

574 vulnerability, and resilience were calculated for floods in the YRDUA and the spatial distribution of

575 flood risks in the region was obtained according to the weights determined by the model. Combined with

576 the natural breakpoint classification method, a flood risk zoning map of the YRDUA was constructed.

577 The extracted flood points were superimposed on the map to verify whether the model exhibited good

578 flood risk assessment capabilities. The results are shown in **Figure 9**, indicating that the distribution of

579 flood points was consistent with the distribution of high and medium-to-high risk areas in the region,

580 with the model assessment results corresponding well with the actual flooding situation. To specifically

581 illustrate the correspondence of the results, the proportion of flood points distributed in high and medium-

582 to-high risk areas was quantitatively calculated. The obtained value was 87.45%, indicating that the flood

583 risk assessment results of the model in this study were highly credible, and subsequent analysis could be

584 conducted.

585 As shown in **Figure 9**, the high and medium-to-high risk areas in the YRDUA were mainly located in the

586 northern part of the region, concentrated in Chizhou, Anqing, Ma'anshan, and Xuancheng Cities in Anhui

587 Province, Yancheng and Yangzhou Cities in Jiangsu Province, and Taizhou City in Zhejiang Province.

588 Meanwhile, most areas of Hangzhou City had the lowest risk. The flood risks in cities such as Shanghai,

Nanjing, and Jinhua were also relatively low. The overall analysis showed that the flood risk in the study area was low in the southwest and high in the northeast, determined largely by natural terrain and meteorological factors. The spatial distribution of the flood hazard class was similar to the distribution of flood risks; exposure decreased stepwise from Shanghai to the surrounding areas, reflecting that densely populated and economically developed cities have higher exposure. Areas with higher vulnerability were mainly concentrated in Chizhou, Anqing, Xuancheng, Chuzhou, and Yancheng Cities. The number of vulnerable people in these cities was relatively high. Vulnerability has aggravated the flood risks in Chizhou and Anqing Cities on the basis of flood risk. Meanwhile, Shanghai had the best resilience performance, followed by those of Hangzhou, Suzhou, and Nanjing Cities, greatly lessening the flood risks in these cities.
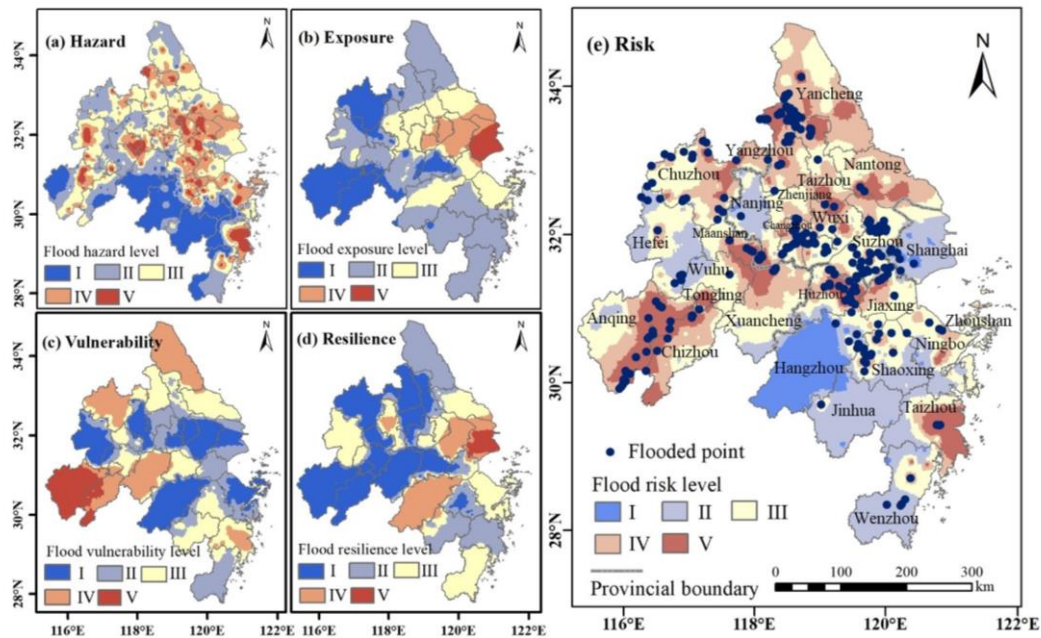
Figure 9: Flood risk level distribution and verification results based on a flood risk assessment model. The flood hazard, exposure, vulnerability, and resilience of the YRDUA were calculated using CatBoost under the AutoML framework and AHP. The flood hazard level (a), flood exposure level (b), flood vulnerability level (c), flood resilience level (d), and flood risk spatial distribution (e) were derived through natural breaks classification in ArcGIS software based on model-determined weights, resulting in a flood risk zoning map for the Yangtze River Delta region.

3.2 Analysis of changes in the spatiotemporal characteristics of flood risk

The flood risk results for the YRDUA from 1990 to 2020 were obtained based on the flood risk assessment model proposed in this study. The differences in flood risk among cities in the YRDUA over

the past few decades are primarily due to a complex interplay of various factors, including geographic and climatic conditions, urbanization processes, socio-economic factors, ecological changes, and historical flood events. The topography and precipitation patterns of different cities affect their capacity for rainwater drainage and accumulation, while urbanization leads to an increase in impervious surfaces and variations in infrastructure development, impacting flood management capabilities. Additionally, differences in DPOP, economic development levels, and flood management policies can exacerbate flood risk. Furthermore, the increasing frequency of extreme weather events due to climate change further elevates flood risk. These factors determine the varying levels of flood risk among cities within the YRDUA.

As the interannual difference in flood risk in the region was small and the change response was weak, we selected the flood risk results for 1990, 2000, 2010, and 2020 to analyze the changes in the spatiotemporal pattern. In this analysis, variables such as PREC and DURA exhibit clear temporal variability, as they change year by year due to weather patterns. However, other factors like DEM, SLOPE, NDVI, and urbanization indicators such as DPOP and GDP are spatial variables that do not exhibit direct temporal changes, but their effects on flood risk are influenced by changing socio-economic and ecological conditions.

Regarding spatial patterns (**Figure 10**), the flood risk in the YRDUA showed clear spatial heterogeneity. The southwestern part of the study area and Shanghai have shown low flood risks over the past 30 years, whereas the central and northern parts of the region have been more likely to face flood risks depending on the natural conditions, population, economic conditions, and recovery capacity of the region. Regarding temporal patterns, from 1990 to 2010, areas with high and medium-to-high risk decreased markedly. By 2010, most of the YRDUA (except for a few areas) was in a state of medium risk or below, with the southwestern region exhibiting a large range of low risk levels. The corresponding areas for each risk level are shown in **Figure 11**. From 1990 to 2010, areas of low and low-to-medium risk levels gradually increased, maximizing in 2010, whereas areas of medium risk and above continued to decrease. By 2020, the number of high-risk areas for flooding increased. There is a tendency for areas of medium-to-high risk in the central region to shift towards high-risk areas in 2020, as compared to the state in 1990. Meanwhile, high-risk areas for floods also appeared in Chizhou and Anqing Cities in Anhui Province, which was mainly due to the intensification of extreme weather, unbalanced population distribution, and rapid economic development in recent years.
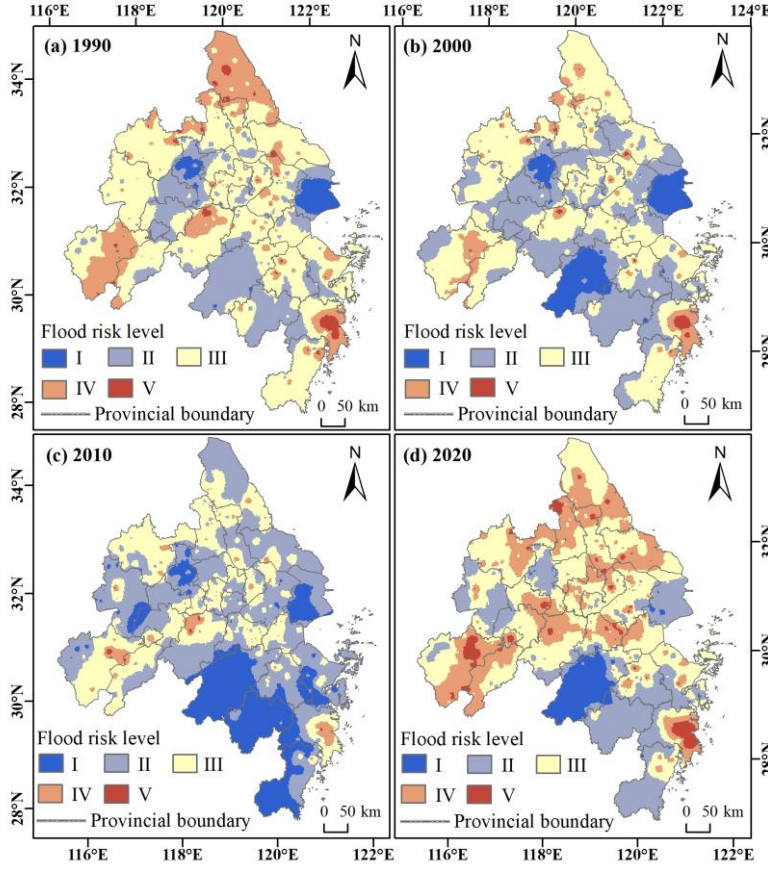
Figure 10: Spatial distributions of flood risk in the YRDUA in different years during 1990–2020.
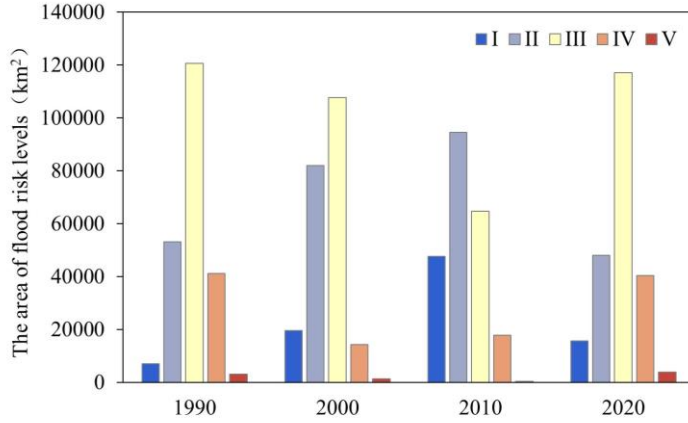
Figure 11: Areas at different levels of flood risk in the YRDUA in different years during 1990–2020.

To further analyze the changes in flood risk in the region, we calculated the change rate of the area of different risk levels every 10 years and the overall change rate over 30 years. The interannual rate of change was expressed in Eq. (13).

$$R_{l,ij} = \frac{Risk_{l,j} - Risk_{l,i}}{Risk_{l,i}} \times 100\%, \tag{13}$$

where $R_{l,ij}$ is the rate of change of the flood risk area of a certain level l in a certain year, i and j are

different years, and $Risk_{l,j}$ and $Risk_{l,j}$ are the areas corresponding to the flood risk of this level in

different years.

The interannual variation rate of the flood risk is shown in **Table 6**. Results showed that the interannual

variation between the areas of low and high risk was relatively large. The low-risk area maximized in

2010, and both R $_{2000-1990}$ and R $_{2010-2000}$ showed a positive variation rate. The high-risk area showed the

largest interannual variation rate from 2010 to 2020, reaching 12.22% and causing the high-risk flood

area in 2020 to spread, resulting in a large high-risk area.

Table 6: Interannual change rates of flood risk areas of different levels (expressed as percentages).

	$R_{2000-1990}$	$R_{2010-2000}$	$R_{2020-2010}$	$R_{2020-1990}$
I	1.77%	1.44%	-0.67%	1.21%
II	0.54%	0.15%	-0.49%	-0.10%
III	-0.11%	-0.40%	0.81%	-0.03%
IV	-0.65%	0.25%	1.25%	-0.02%
V	-0.53%	-0.80%	12.22%	0.27%

Analyzing the flood risk of the entire urban agglomeration does not reveal the spatial scale effect of flood

risk, nor does it consider the correlation and impact of flood risk at different spatial scales. To reflect the

distribution of and changes in flood risk at different spatial scales within the region, the risk intensity of

different provinces was further analyzed, and the results are shown in **Figure 12**, respectively. In **Figure

12**, the average flood risk reflects the differences in risk development of the provincial administrative

units in Shanghai, Anhui, Zhejiang, and Jiangsu in terms of time and space. Overall, all administrative

units in the YRDUA exhibited the highest flood risk in 2020, and the overall risk trend increased. At the

provincial level, Shanghai's flood risk was consistently low, showing a trend of first decreasing from

0.152 in 1990 to 0.123 in 2000 and then gradually increasing to 0.311 in 2020. Among the other three

provinces, Jiangsu and Anhui had relatively high flood risks, reaching 0.525 and 0.516, respectively, in

2020, whereas Zhejiang had a relatively low flood risk, which remained stable between 1990 and 2010,

with no distinct changes.

672
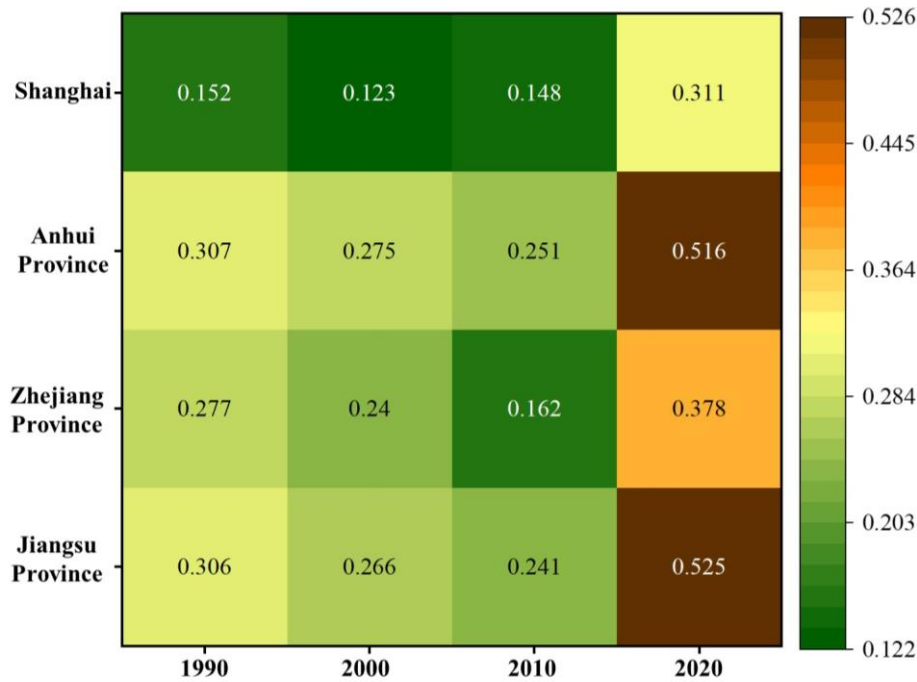
Figure 12: Distribution of Average Flood Risk in Each Province of the Yangtze River Delta Urban Agglomeration from 1990 to 2020

675

4 Conclusion

Flood risk assessment at the scale of urban agglomeration is a hot research topic in the field of disaster prevention and mitigation. In this study, the flood risk assessment indexes for YRDUA were determined in different dimensions of danger, exposure, vulnerability and resilience, and a flood risk assessment model based on AutoML and AHP was constructed to study the changes of spatial and temporal characteristics of flood risk in the region in the last 30 years from 1990 to 2020, aiming to provide scientific basis for the prevention and resilience of the YRDUA. The main conclusions of this study are as follows:

(1) In the flood risk calculation, the CatBoost model has the highest Precision, F1-score, and Kappa, and its Precision can reach 0.9030. Further analysis of the ROC curve and the corresponding AUC value of the model shows that its AUC value is 0.91, which indicates that the CatBoost model has the best performance and prediction reliability. Therefore, the CatBoost model was selected to calculate the flood risk in the YRDUA.

(2) Using the flood risk assessment model based on AutoML and AHP to obtain the flood risk of the YRDUA, superimposed on the flooded point data for comparative analysis, we found that the distribution of flooded points in the study area is basically consistent with the distribution of high and medium-to-high risk areas of flooding, and the proportion of the distribution of the quantification of its distribution is 87.45%, which indicates that the model in this study has a good performance and credibility regarding the assessment of flood risk.

(3) The spatial distribution of flood risk in the YRDUA during the 30-year study period shows obvious heterogeneity, with the southwestern part of the region and Shanghai City having a low flood risk, whereas the north-central part of the region faces a relatively high probability of flood risk. Between 1990 and 2010, there was a substantial decrease in the high and medium-to-high risk flood zones; yet by 2020, there was an increase in the high-risk flood zones. There is a tendency for the medium-to-high risk area in the center of the region to shift to a high-risk area, whereas high-risk areas also occur in the cities of Chizhou and Anqing in Anhui Province.

(4) All administrative units of the YRDUA exhibited the highest flood risk in 2020, with an overall trend of increasing risk. At the provincial level, Jiangsu and Anhui Provinces possess relatively high flood risks, whereas Zhejiang Province has a relatively low flood risk.

(5) The findings of this study provide valuable insights for flood risk management and policy-making. The flood risk maps generated in this study can serve as a scientific basis for urban planning, infrastructure development, emergency response, and disaster prevention strategies. By integrating these risk assessments into decision-making processes, government agencies and urban planners can optimize flood prevention measures and enhance regional resilience. Furthermore, the AutoML framework used in this study can be applied to other regions for flood risk assessment and can be integrated with future climate change scenarios to enable long-term forecasting and proactive disaster mitigation strategies.

Data availability.

Administrative boundaries and river network density were obtained from the Resource and Environmental Science and Data Center, Chinese Academy of Sciences (https://www.resdc.cn/DataList.aspx). Digital elevation data were derived from the SRTM1 dataset provided by USGS (https://earthexplorer.usgs.gov/). Land use data were sourced from the China Land

Cover Dataset (CLCD) developed by Wuhan University (https://zenodo.org/records/8176941). Hourly

precipitation data from 120 meteorological stations were obtained from the National Meteorological

Information Center, China Meteorological Administration (https://data.cma.cn/). Historical flood

inundation data were obtained from the MODIS-based Global Flood Database and validated using the

EM-DAT   disaster   database

(https://developers.google.com/earthengine/datasets/catalog/GLOBAL_FLOOD_DB_MODIS_EVENT

S_V1).

Competing interests.

The authors declare that they have no competing financial interests or personal relationships that may

have influenced the work reported in this study.

Author contributions.

YG: Writing - original draft preparation, Validation, Software, Methodology, Conceptualization **HL:**
Writing-review & editing, Visualization, Supervision, Formal analysis. **YZ:** Methodology, Formal
analysis. **HJ:** Writing - review & editing, Methodology. **SW:** Software, Formal analysis. **YG:**
Visualization, Software. **SZ:** Writing-review & editing, Resources, Project administration, Funding
acquisition, Conceptualization .

Acknowledgements

This study was supported by the National Natural Science Foundation of China (Grant Nos. 42271483
and 42071364) and Jiangsu Provincial Natural Resources Science and Technology Project
(JSZRKJ202405). We would like to thank Editage (www.editage.cn) for English language editing.

References

Abu-Salih, B., Wongthongtham, P., Coutinho, K., Qaddoura, R., Alshaweesh, O., and Wedyan, M.: The
development of a road network flood risk detection model using optimised ensemble learning, Eng. Appl.
Artif. Intell., 122, 106081, https://doi.org/10.1016/j.engappai.2023.106081, 2023.

741 Adnan, R. M., Yuan, X., Kisi, O., and Anam, R.: Improving Accuracy of River Flow Forecasting Using

742 LSSVR with Gravitational Search Algorithm, Advances in Meteorology, 2017, 1–23,

743 https://doi.org/10.1155/2017/2391621, 2017.

744 Anon: Identification of sensitivity indicators of urban rainstorm flood disasters: A case study in China,

745 J. Hydrology., 599, 126393, https://doi.org/10.1016/j.jhydrol.2021.126393, 2021.

746 Aven, T.: Risk assessment and risk management: Review of recent advances on their foundation,

747 European Journal of Operational Research, 253, 1–13, https://doi.org/10.1016/j.ejor.2015.12.023, 2016.

748 Bostan, P. A., Heuvelink, G. B. M., and Akyurek, S. Z.: Comparison of regression and kriging techniques

749 for mapping the average annual precipitation of Turkey, Int. J. Appl. Earth Obs. Geoinf., 19, 115–126,

750 https://doi.org/10.1016/j.jag.2012.04.010, 2012.

751 Consuegra-Ayala, J. P., Gutiérrez, Y., Almeida-Cruz, Y., and Palomar, M.: Intelligent ensembling of

752 auto-ML system outputs for solving classification problems, Inform. Sci., 609, 766–780,

753 https://doi.org/10.1016/j.ins.2022.07.061, 2022.

754 Cressie, N.: The origins of kriging, Math Geol, 22, 239–252, https://doi.org/10.1007/BF00889887, 1990.

755 Criado, M., Martínez-Graña, A., San Román, J. S., and Santos-Francés, F.: Flood risk evaluation in urban

756 spaces: The study case of Tormes River (Salamanca, Spain), International journal of environmental

757 research and public health, 16, 5, 2019.

758 Ding, T., Chen, J., Fang, Z., and Chen, J.: Assessment of coordinative relationship between

759 comprehensive ecosystem service and urbanization: A case study of Yangtze River Delta urban

760 Agglomerations, China, Ecol. Indic., 133, 108454, https://doi.org/10.1016/j.ecolind.2021.108454, 2021.

761 Donegan, H. A., Dodd, F. J., and McMaster, T. B. M.: A New Approach to Ahp Decision-Making,

762 Journal of the Royal Statistical Society: Series D (The Statistician), 41, 295–302,

763 https://doi.org/10.2307/2348551, 1992.

764 Echendu, A. J.: The impact of flooding on Nigeria's sustainable development goals (SDGs), Ecosyst.

765 Health Sustainability, 6, 1791735, https://doi.org/10.1080/20964129.2020.1791735, 2020.

766 Fernández, D. S. and Lutz, M. A.: Urban flood hazard zoning in Tucumán Province, Argentina, using

767 GIS and multicriteria decision analysis, Eng. Geol., 111, 90–98, 2010.

768 Gain, A. K., Mojtahed, V., Biscaro, C., Balbi, S., and Giupponi, C.: An integrated approach of flood risk

769 assessment in the eastern part of Dhaka City, Nat. Hazards, 79, 1499–1530,

770 https://doi.org/10.1007/s11069-015-1911-7, 2015.

771 Gu, C., Hu, L., Zhang, X., Wang, X., and Guo, J.: Climate change and urbanization in the Yangtze River

772 Delta, Habitat Int., 35, 544–552, https://doi.org/10.1016/j.habitatint.2011.03.002, 2011.

773 Guan, X., Yu, F., Xu, H., Li, C., and Guan, Y.: Flood risk assessment of urban metro system using

774 random forest algorithm and triangular fuzzy number based analytical hierarchy process approach,

775 Sustainable Cities and Society, 109, 105546, https://doi.org/10.1016/j.scs.2024.105546, 2024.

776 Gudiyangada Nachappa, T., Tavakkoli Piralilou, S., Gholamnia, K., Ghorbanzadeh, O., Rahmati, O., and

777 Blaschke, T.: Flood susceptibility mapping with machine learning, multi-criteria decision analysis and

778 ensemble using Dempster Shafer Theory, Journal of Hydrology, 590, 125275,

779 https://doi.org/10.1016/j.jhydrol.2020.125275, 2020.

780 Guo, Y., Quan, L., Song, L., and Liang, H.: Construction of rapid early warning and comprehensive

781 analysis models for urban waterlogging based on AutoML and comparison of the other three machine

782 learning algorithms, J. Hydrol., 605, 127367, 2022a.

783 Guo, Y., Quan, L., Song, L., and Liang, H.: Construction of rapid early warning and comprehensive

784 analysis models for urban waterlogging based on AutoML and comparison of the other three machine

785 learning algorithms, J. Hydrol., 605, 127367, https://doi.org/10.1016/j.jhydrol.2021.127367, 2022b.

786 Guo, Y., Quan, L., Song, L., and Liang, H.: Construction of rapid early warning and comprehensive

787 analysis models for urban waterlogging based on AutoML and comparison of the other three machine

788 learning algorithms, Journal of Hydrology, 605, 127367, https://doi.org/10.1016/j.jhydrol.2021.127367,

789 2022c.

790 He, X., Zhao, K., and Chu, X.: AutoML: A survey of the state-of-the-art, Knowledge-Based Systems,

791 212, 106622, https://doi.org/10.1016/j.knosys.2020.106622, 2021a.

792 He, X., Zhao, K., and Chu, X.: AutoML: A survey of the state-of-the-art, Knowledge-Based Systems,

793 212, 106622, https://doi.org/10.1016/j.knosys.2020.106622, 2021b.

794 Hites, R., De Smet, Y., Risse, N., Salazar-Neumann, M., and Vincke, P.: About the applicability of

795 MCDA to some robustness problems, European Journal of Operational Research, 174, 322–332,

796 https://doi.org/10.1016/j.ejor.2005.01.031, 2006.

797 Hsiao, S.-C., Chiang, W.-S., Jang, J.-H., Wu, H.-L., Lu, W.-S., Chen, W.-B., and Wu, Y.-T.: Flood risk

798 influenced by the compound effect of storm surge and rainfall under climate change for low-lying coastal

799 areas, Science of the total environment, 764, 144439, 2021.

Hutter, F., Kotthoff, L., and Vanschoren, J. (Eds.): Automated Machine Learning: Methods, Systems, Challenges, Springer Nature, https://doi.org/10.1007/978-3-030-05318-5, 2019.

Jordan, M. and Mitchell, T.: Machine learning: Trends, perspectives, and prospects, Science, 349, 255–260, https://doi.org/10.1126/science.aaa8415, 2015.

Kanani-Sadat, Y., Arabsheibani, R., Karimipour, F., and Nasseri, M.: A new approach to flood susceptibility assessment in data-scarce and ungauged regions based on GIS-based hybrid multi criteria decision-making method, J. Hydrol., 572, 17–31, https://doi.org/10.1016/j.jhydrol.2019.02.034, 2019.

Kazienko, P., Lughofer, E., and Trawinski, B.: Editorial on the special issue "Hybrid and ensemble techniques in soft computing: recent advances and emerging trends," Soft Computing., 19, 3353–3355, https://doi.org/10.1007/s00500-015-1916-x, 2015.

Khadka, D., Babel, M. S., and Kamalamma, A. G.: Assessing the Impact of Climate and Land-Use Changes on the Hydrologic Cycle Using the SWAT Model in the Mun River Basin in Northeast Thailand, Water, 15, 3672, https://doi.org/10.3390/w15203672, 2023.

Khosravi, K., Shahabi, H., Pham, B. T., Adamowski, J., Shirzadi, A., Pradhan, B., Dou, J., Ly, H.-B., Gróf, G., Ho, H. L., Hong, H., Chapi, K., and Prakash, I.: A comparative assessment of flood susceptibility modeling using Multi-Criteria Decision-Making Analysis and Machine Learning Methods, J. Hydrol., 573, 311–323, https://doi.org/10.1016/j.jhydrol.2019.03.073, 2019.

Lang, M., Barriendos, M., Llasat, M. C., Francés, F., Ouarda, T., Thorndycraft, V., Enzel, Y., Bardossy, A., Coeur, D., and Bobée, B.: Use of Systematic, Palaeoflood and Historical Data for the Improvement of Flood Risk Estimation. Review of Scientific Methods, Nat. Hazards, 31, 623–643, https://doi.org/10.1023/B:NHAZ.0000024895.48463.eb, 2004.

Li, J., Cheng, K., Wang, S., Morstatter, F., Trevino, R. P., Tang, J., and Liu, H.: Feature Selection: A Data Perspective, ACM Comput. Surv., 50, 94:1-94:45, https://doi.org/10.1145/3136625, 2017.

Lin, L., Wu, Z., and Liang, Q.: Urban flood susceptibility analysis using a GIS-based multi-criteria analysis framework, Nat Hazards, 97, 455–475, https://doi.org/10.1007/s11069-019-03615-2, 2019.

Liu Jiafu and Zhang Bai: Progress of Rainstorm Flood Risk Assessment, Geographical Science, 35, 346–351, https://doi.org/10.13249/j.cnki.sgs.2015.03.013, 2015.

Lu, H., Lu, X., Jiao, L., and Zhang, Y.: Evaluating urban agglomeration resilience to disaster in the Yangtze Delta city group in China, Sustainable Cities and Society, 76, 103464, 2022.

829 Lundberg, S. M. and Lee, S.-I.: A Unified Approach to Interpreting Model Predictions, in: Advances in

830 Neural Information Processing Systems, 2017.

831 Ma, C., Chen, Z., Zhao, K., Xu, H., and Qi, W.: Improved urban flood risk assessment based on

832 spontaneous-triggered risk assessment conceptual model considering road environment, Journal of

833 Hydrology, 608, 127693, https://doi.org/10.1016/j.jhydrol.2022.127693, 2022.

834 Mahmoud, S. H. and Gan, T. Y.: Urbanization and climate change implications in flood risk management:

835 Developing an efficient decision support system for flood susceptibility mapping, Science of The Total

836 Environment, 636, 152–167, https://doi.org/10.1016/j.scitotenv.2018.04.282, 2018.

837 Mia, Md. U., Rahman, M., Elbeltagi, A., Abdullah-Al-Mahbub, Md., Sharma, G., Islam, H. M. T., Pal,

838 S. C., Costache, R., Islam, A. R. Md. T., Islam, M. M., Chen, N., Alam, E., and Washakh, R. M. A.:

839 Sustainable flood risk assessment using deep learning-based algorithms with a blockchain technology,

840 Geocarto International, 38, 1–29, https://doi.org/10.1080/10106049.2022.2112982, 2023.

841 Milanesi, L., Pilotti, M., and Ranzi, R.: A conceptual model of people's vulnerability to floods, Water

842 Resources Res., 51, 182–197, https://doi.org/10.1002/2014WR016172, 2015.

843 Mirzaei, S., Vafakhah, M., Pradhan, B., and Alavi, S. J.: Flood susceptibility assessment using extreme

844 gradient boosting (EGB), Iran, Earth Sci. Inf., 14, 51–67, https://doi.org/10.1007/s12145-020-00530-0,

845 2021.

846 Mishra, K. and Sinha, R.: Flood risk assessment in the Kosi megafan using multi-criteria decision

847 analysis: A hydro-geomorphic approach, Geomorphology, 350, 106861,

848 https://doi.org/10.1016/j.geomorph.2019.106861, 2020.

849 Morales-Torres, A., Escuder-Bueno, I., Andrés-Doménech, I., and Perales-Momparler, S.: Decision

850 Support Tool for energy-efficient, sustainable and integrated urban stormwater management,

851 Environmental Modelling & Software, 84, 518–528, https://doi.org/10.1016/j.envsoft.2016.07.019, 2016.

852 Munim, Z. H., Sørli, M. A., Kim, H., and Alon, I.: Predicting maritime accident risk using Automated

853 Machine Learning, Reliab. Eng. Syst. Saf., 248, 110148, https://doi.org/10.1016/j.ress.2024.110148,

854 2024.

855 Nagarajah, T. and Poravi, G.: A Review on Automated Machine Learning (AutoML) Systems, in: 2019

856 IEEE 5th International Conference for Convergence in Technology (I2CT), 2019 IEEE 5th International

857 Conference for Convergence in Technology (I2CT), 1–6,

858 https://doi.org/10.1109/I2CT45611.2019.9033810, 2019.

859 Nayak, P. C., Sudheer, K. P., Rangan, D. M., and Ramasastri, K. S.: A neuro-fuzzy computing technique

860 for modeling hydrological time series, J. Hydrol., 291, 52–66, 2004.

861 Özdemir, H., Baduna Koçyiğit, M., and Akay, D.: Flood susceptibility mapping with ensemble machine

862 learning: a case of Eastern Mediterranean basin, Türkiye, Stoch. Env. Res. Risk A., 37, 4273–4290,

863 https://doi.org/10.1007/s00477-023-02507-z, 2023.

864 Pham, B. T., Luu, C., Dao, D. V., Phong, T. V., Nguyen, H. D., Le, H. V., von Meding, J., and Prakash,

865 I.: Flood risk assessment using deep learning integrated with multi-criteria decision analysis, Knowledge-

866 Based Systems, 219, 106899, https://doi.org/10.1016/j.knosys.2021.106899, 2021.

867 Raschka, S.: Model Evaluation, Model Selection, and Algorithm Selection in Machine Learning,

868 https://doi.org/10.48550/arXiv.1811.12808, 10 November 2020.

869 Rashidi Shikhteymour, S., Borji, M., Bagheri-Gavkosh, M., Azimi, E., and Collins, T. W.: A novel

870 approach for assessing flood risk with machine learning and multi-criteria decision-making methods,

871 Appl. Geogr., 158, 103035, https://doi.org/10.1016/j.apgeog.2023.103035, 2023.

872 Saaty, T. L.: The Analytic Hierarchy Process: Decision Making in Complex Environments, in:

873 Quantitative Assessment in Arms Control: Mathematical Modeling and Simulation in the Analysis of

874 Arms Control Problems, edited by: Avenhaus, R. and Huber, R. K., Springer US, Boston, MA, 285–308,

875 https://doi.org/10.1007/978-1-4613-2805-6_12, 1984.

876 Sarro, F., Moussa, R., Petrozziello, A., and Harman, M.: Learning From Mistakes: Machine Learning

877 Enhanced Human Expert Effort Estimates, IEEE Trans. Softw. Eng., 48, 1868–1882,

878 https://doi.org/10.1109/TSE.2020.3040793, 2022.

879 Scott, D., Hall, C. M., Rushton, B., and Gössling, S.: A review of the IPCC Sixth Assessment and

880 implications for tourism development and sectoral climate action, J. Sustain. Tour., 0, 1–18,

881 https://doi.org/10.1080/09669582.2023.2195597, 2023.

882 Seemuangngam, A. and Lin, H.-L.: The impact of urbanization on urban flood risk of Nakhon

883 Ratchasima, Thailand, Appl. Geogr., 162, 103152, https://doi.org/10.1016/j.apgeog.2023.103152, 2024.

884 Shafizadeh-Moghadam, H., Valavi, R., Shahabi, H., Chapi, K., and Shirzadi, A.: Novel forecasting

885 approaches using combination of machine learning and statistical models for flood susceptibility

886 mapping, Journal of environmental management, 217, 1–11, 2018.

887 Shuster, W. D., Bonta, J., Thurston, H., Warnemuende, E., and Smith, D. R.: Impacts of impervious

888 surface on watershed hydrology: A review, Urban Water Journal,

889 https://doi.org/10.1080/15730620500386529, 2005.

890 Sinha, R., Bapalu, G. V., Singh, L. K., and Rath, B.: Flood risk analysis in the Kosi river basin, north

891 Bihar using multi-parametric approach of Analytical Hierarchy Process (AHP), J. Indian Soc. Remote

892 Sens., 36, 335–349, https://doi.org/10.1007/s12524-008-0034-y, 2008.

893 Sun, B., Fang, C., Liao, X., Guo, X., and Liu, Z.: The relationship between urbanization and air pollution

894 affected by intercity factor mobility: A case of the Yangtze River Delta region, Environ. Impact Assess.

895 Rev., 100, 107092, https://doi.org/10.1016/j.eiar.2023.107092, 2023.

896 Tang, Z., Wang, P., Li, Y., Sheng, Y., Wang, B., Popovych, N., and Hu, T.: Contributions of climate

897 change and urbanization to urban flood hazard changes in China's 293 major cities since 1980, J. Environ.

898 Manage., 353, 120113, https://doi.org/10.1016/j.jenvman.2024.120113, 2024.

899 Vincent, A. M., K.s.s., P., and Jidesh, P.: Flood susceptibility mapping using AutoML and a deep learning

900 framework with evolutionary algorithms for hyperparameter optimization, Applied Soft Computing., 148,

901 110846, https://doi.org/10.1016/j.asoc.2023.110846, 2023.

902 Wagenaar, D., Curran, A., Balbi, M., Bhardwaj, A., Soden, R., Hartato, E., Mestav Sarica, G., Ruangpan,

903 L., Molinario, G., and Lallemant, D.: Invited perspectives: How machine learning will change flood risk

904 and impact assessment, Nat. Hazard. Earth Sys., 20, 1149–1161, https://doi.org/10.5194/nhess-20-1149-

905 2020, 2020.

906 Wan, H., Zhong, Z., Yang, X., and Li, X.: Impact of city belt in Yangtze River Delta in China on a

907 precipitation process in summer: A case study, Atmos. Res., 125–126, 63–75,

908 https://doi.org/10.1016/j.atmosres.2013.02.004, 2013.

909 Wang, M., Fu, X., Zhang, D., Chen, F., Liu, M., Zhou, S., Su, J., and Tan, S. K.: Assessing urban flooding

910 risk in response to climate change and urbanization based on shared socio-economic pathways, Science

911 of The Total Environment, 880, 163470, https://doi.org/10.1016/j.scitotenv.2023.163470, 2023a.

912 Wang, P., Deng, X., Zhou, H., and Qi, W.: Responses of urban ecosystem health to precipitation extreme:

913 A case study in Beijing and Tianjin, Journal of Cleaner Production, 177, 124–133,

914 https://doi.org/10.1016/j.jclepro.2017.12.125, 2018a.

Wang, P., Li, Y., Yu, P., and Zhang, Y.: The analysis of urban flood risk propagation based on the modified susceptible infected recovered model, J. Hydrology., 603, 127121, https://doi.org/10.1016/j.jhydrol.2021.127121, 2021.

Wang, T., Wang, H., Wang, Z., and Huang, J.: Dynamic risk assessment of urban flood disasters based on functional area division—A case study in Shenzhen, China, J. Environ. Manage., 345, 118787, https://doi.org/10.1016/j.jenvman.2023.118787, 2023b.

Wang, Y., Liu, G., Guo, E., and Yun, X.: Quantitative Agricultural Flood Risk Assessment Using Vulnerability Surface and Copula Functions, Water, 10, 1229, https://doi.org/10.3390/w10091229, 2018b.

Wang, Y., Li, C., Hu, Y., Lv, J., Liu, M., Xiong, Z., and Wang, Y.: Evaluation of urban flooding and potential exposure risk in central and southern Liaoning urban agglomeration, China, Ecological Indicators, 154, 110845, https://doi.org/10.1016/j.ecolind.2023.110845, 2023c.

Webb, G. I. and Zheng, Z.: Multistrategy ensemble learning: reducing error by combining ensemble learning techniques, IEEE Transactions on Knowledge and Data Engineering, 16, 980–991, https://doi.org/10.1109/TKDE.2004.29, 2004.

Webster, R. and Oliver, M. A.: Geostatistics for Environmental Scientists, John Wiley & Sons, 333 pp., 2007.

Wolpert, D. H. and Macready, W. G.: No free lunch theorems for optimization, IEEE Transactions on Evolutionary Computation, 1, 67–82, https://doi.org/10.1109/4235.585893, 1997.

Xu, H., Hou, X., Pan, S., Bray, M., and Wang, C.: Socioeconomic impacts from coastal flooding in the 21st century China's coastal zone: A coupling analysis between coastal flood risk and socioeconomic development, Sci. Total Environ., 917, 170187, 2024.

Yan, M., Yang, J., Ni, X., Liu, K., Wang, Y., and Xu, F.: Urban waterlogging susceptibility assessment based on hybrid ensemble machine learning models: A case study in the metropolitan area in Beijing, China, J. Hydrol., 630, 130695, 2024.

Yang, J., Zeng, X., Zhong, S., and Wu, S.: Effective Neural Network Ensemble Approach for Improving Generalization Performance, IEEE Transactions on Neural Networks and Learning Systems, 24, 878–887, https://doi.org/10.1109/TNNLS.2013.2246578, 2013.

943   Yang, W., Xu, K., Lian, J., Ma, C., and Bin, L.: Integrated flood vulnerability assessment approach based

944   on TOPSIS and Shannon entropy methods, Ecol. Indic., 89, 269–280,

945   https://doi.org/10.1016/j.ecolind.2018.02.015, 2018.

946   Yang, X., Li, H., Zhang, J., Niu, S., and Miao, M.: Urban economic resilience within the Yangtze River

947   Delta urban agglomeration: Exploring spatially correlated network and spatial heterogeneity, Sustainable

948   Cities and Society, 103, 105270, https://doi.org/10.1016/j.scs.2024.105270, 2024.

949   Yuan, X., Chen, C., Lei, X., Yuan, Y., and Muhammad Adnan, R.: Monthly runoff forecasting based on

950   LSTM–ALO model, Stoch. Env. Res. Risk A., 32, 2199–2212, https://doi.org/10.1007/s00477-018-

951   1560-y, 2018.

952   Zhang, H., Wu, C., Chen, W., and Huang, G.: Assessing the Impact of Climate Change on the

953   Waterlogging Risk in Coastal Cities: A Case Study of Guangzhou, South China,

954   https://doi.org/10.1175/JHM-D-16-0157.1, 2017.

955